To study the Mueller matrix polarimetry for the characterization of wood and Teflon flat samples

Sidra Batool [a,c,*], Mehwish Nisar [a,c], Fabio Mangini [a,b], Fabrizio Frezza [a,c], Eugenio Fazio [a,c]

[a] Department of Information Engineering, Electronics and Telecommunications, "La Sapienza" University of Rome, Via Eudossiana 18, 00184 Rome, Italy
[b] Department of information Engineering, University of Brescia, Italy
[c] Department of Fundamental and Applied Sciences for Engineering, Sapienza University of Rome, Via A. Scarpa 16, 00161 Roma, Italy

ARTICLE INFO

ABSTRACT

In our manuscript, we carry out the Mueller matrix polarimetry for the characterization of wood and polytetrafluoroethylene (PTFE) or Teflon flat samples. Polarization measurements allows to enhance the imaging contrast of the anisotropic wood (Horizontal (H) and Vertical (V)) superficial fibers tissues and isotropic material (Teflon). We study the polarization-sensitive parameters for better investigations of the micro- and macrostructural and optical properties of complex tissues. The polarization imaging methodology has evolved to accept increasingly complex parametric measurements. The Mueller matrix is now generally calculated using a polarimetry technique. Herein, we attempt to study the difference between wood H, wood V, and Teflon samples. We calculated 3×3 Mueller matrix, which can be used to describe an intuitive overview of the material characteristics. We have interpreted our experimental results of Mueller matrix coefficients in terms of graphical representation using two different approaches named MS_1 and MS_2. This study gives us a new idea on the contrast mechanisms of polarization-sensitive measurements for different samples wood H, wood V, and Teflon and may provide new and simple diagnostic techniques for biological applications.

1. Introduction

The advancement of biomedical diagnostic optical techniques is significant current research interest, as optical methods can promote non-invasive and quantitative diagnosis (Liu et al., 1992; Vo, 2014; Fujimoto and Farkas, 2009; Batool et al., 2020c). For optical analysis, the Mueller matrix polarimetric techniques are commonly used for the characterization of the biological tissues (Tuchin, 2016; Alali and Vitkin, 2015). The polarization parameters of light reflected from anisotropic sample (wood) and isotropic sample (Teflon) are useful for the morphological information in the biomedical field. But optical inspection of the isotropic/ anisotropic samples faces formidable challenges due to multiple scattering events and numerical elaboration of measurements with different polarizations in terms of unique and authentic interpretation of the Mueller matrix for biological diagnostics (Saarinen and Muinonen, 2011; Kienle et al., 2008).

In biomedical diagnosis (Batool et al., 2020d; , Batool et al., 2021a), polarimetric methods have also gained more attention recently, because the polarization of light scattering from the fibrous tissues provides additional diagnostic details that can not be derived

from the blind polarization measurements. For example, the anisotropic material samples with their fibrous structure lead to the phenomena of linear birefringence (or linear retardance). Similarly, muscle fibers and protein collagens possess fibrous structure also demonstrate linear birefringence. The optical birefringence properties are changed by changes in the fibrous structure from disease development or treatment response, making this a potentially responsive tissue status probe (Zaffar and Pradhan, 2020; Yu et al., 2020; Gurjar et al., 2001). The Mueller matrix expresses the transfer function of an optical system, after its interactions with polarized light. It contains all information about the polarization properties and characteristics of the samples (Gurjar et al., 2001). We have been investigating the use of an expanded Mueller matrix interpretational approach to the polarimetry characteristics of the tissues can be potentially serve as a useful biological treatment.

In the last decade, the scattering applications (Batool et al., 2020a; Mangini and Tedeschi, 2017; Batool et al., 2020b, 2018) have achieved great progress for the investigation of biological structures (Fratzl et al., 1997). It can push for more complex structural characterization of the material based on biomedical diagnostic techniques

* Corresponding author at: Department of Information Engineering, Electronics and Telecommunications, "La Sapienza" University of Rome, Via Eudossiana 18, 00184 Rome, Italy. Tel.: +393335045995.
E-mail address: sidra.batool@uniroma1.it (S. Batool).

including polarization imaging and spectroscopy, amplitude and intensity of light scattering matrix measurements and polarization-sensitive optical coherence tomography (De Boer and Milner, 2002). The polarization optical methods are essential quantitative studies in biomedical diagnostics. The fibrous tissues can analyzed with the corresponding models showing linear and circular birefringence, dichroism and, chirality (Johnson and Guy, 1972).

Optical polarization imaging is popular convenient non-invasive technique for the detection of biological structures. The ultimate goal is the detection of millimeter-sized small tissues in the biological texture (Jacques et al., 2016; Jiao and Wang, 2002; Layden et al., 2013). Demos and Staggs (2006) reported techniques regarding polarization principles for non-invasive surface imaging of biological systems. Polarization discrimination of scattered photons was precisely used employing a non-rotating retarder polarimetric configuration to enhance the visualization of the subsurface textures. Jacques et al. (2009) used the simple polarization principle for visualizing superficial layers of tissue such as skin, breast, brain, bones, connective tissue, and fat. Saarinen and Muinonen (2011) investigated the scattering of light using wood fibers. The components of the reflected light from the wood fibers contained information regarding its structure. They described the wood-fiber absorption, scattering cross-sections, and scattering matrices in the ray-optics approximation. They observed the complicated internal structure of the wood fibers.

In this manuscript, we study the calculation of the Mueller matrix coefficient for samples of wood (H and V orientation of fibers) and Teflon. We are considering wood (wood-H and wood-V) as different anisotropic material samples and Teflon as an isotropic material samples. For this, we need a realistic experimental polarization imaging approach for material identification and comparison between the wood (H-V) and Teflon samples. The ultimate goal of this study is to express the optical behavior of veins, arteries, and nerves for the biomedical diagnosis. For the sake of simplicity, we investigated flat objects such as wood and Teflon in order to understand thoroughly the light scattering effects for its material characteristics. We are assuming that the characteristic features of wood (H-V) may be associated to nerves and arteries respectively and characteristic features of Teflon may be associated to veins shown in Fig. 1.

In the future, we will study the light scattering effects and Mueller matrix characteristic features using circular-shaped object. After collecting complete background knowledge of the optical properties of light with cylindrical rod shape object, we will investigate the optical behavior of nerves, arteries, and veins.

2. Experimental setup

Wood (H-V oriented) and Teflon samples have been illuminated by linearly polarized light shown in Fig. 2. The wavelength of illumination is 450 nm from a LED, which is collimated by a lens L_1 and then propagates through a linear polarizer P_1. The samples were illuminated orthogonally, observed at different large angles in order to see the behavior of light according to the respective angle. Backscattered light in terms of photons from the sample passes through the lens L_2 and second polarizer P_2. Finally, images were captured by a camera, which is connected to the computer. The images were mathematically inspected, to determine the properties of the light diffused towards the observer. In our experimental setup, both polarizers P_1 and P_2 can rotate around their optical axis to vary polarization angles for illumination θ_i and detection θ_s shown in Figs. 3 and 4.

2.1. Methodology scheme $(MS)_1$

We captured a series of images $I(\theta_i, \theta_s)$, for incident polarization set of angles $\{315°, 0°, 45°, 90°\}$ using P_1. We took four images by setting P_2 at $\{315°, 0°, 45°, 90°\}$ corresponding to each incident polarization. In this way, we recorded sixteen images for each sample with respect to different angles of observation. Methodology Scheme MS_1 illustrated in Figs. 5, 6 and Table 1. Meanwhile first polarizer P_1 has been removed from our experimental setting, we took again four images by rotating the second polarizer P_2 according to the set of angles $\{315°, 0°, 45°, 90°\}$. We embedded the first polarizer P_1 and removed the second polarizer in the experimental setup, we took four images using the first polarizer P_1 with same set of angles. Finally, we captured one image without using both polarizers P_1 and P_2. This descrip-

(a) wood   (b) Teflon
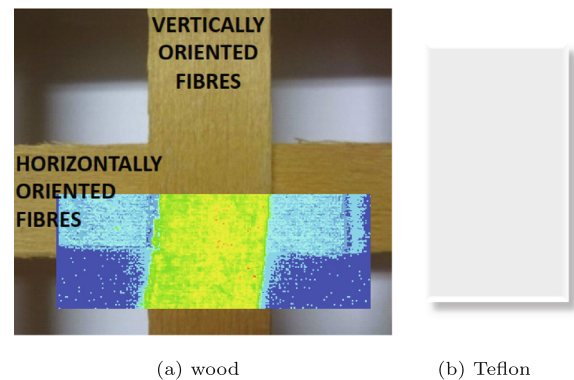
Fig. 2. Representation of wood-H, wood-V, and Teflon samples.
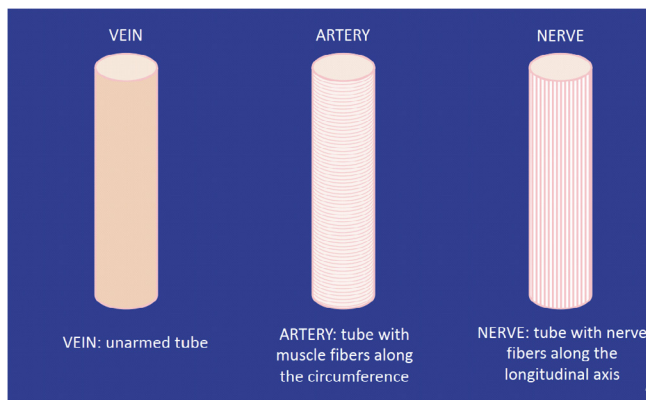
Fig. 1. Characterization of biological samples (veins, arteries, and nerves).
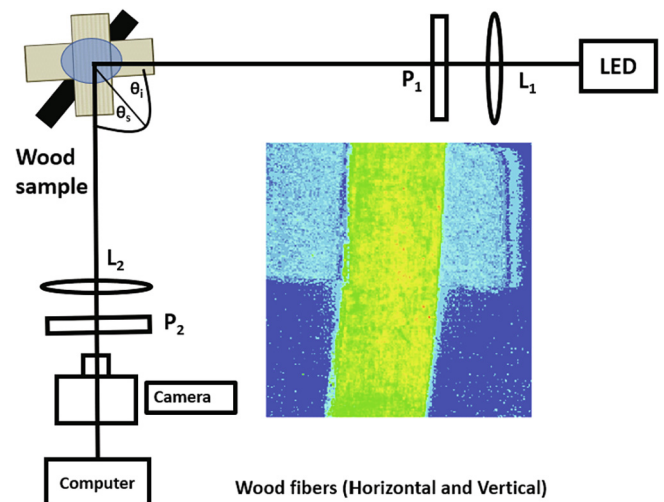
Fig. 3. Experimental setup.
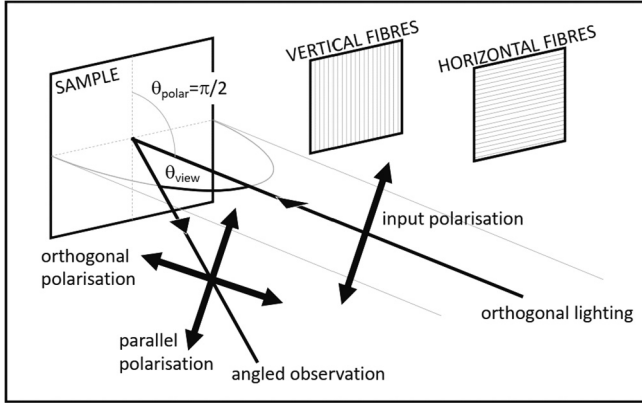
Fig. 4. Experimental geometry. A sample is orthogonally illuminated by incoherent linearly polarized light. A camera records images of the sample surface at different azimuthal angles θ_{view}, performing a selection of the observed light polarizations, both parallel and orthogonal to the input one.
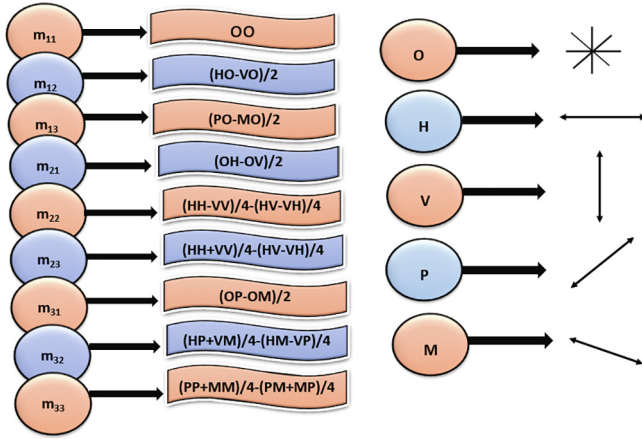
Fig. 5. Formation of Mueller matrix elements for MS_1.

tion is for N in Table 1. In this way, we recorded total of twenty-five images for all samples.

2.2. Methodology scheme $(MS)_2$

Here wood-H, wood-V, and Teflon samples have been investigated with alternative speculation. We considered the same experimental setup, but the formation of Mueller matrix is different. For this purpose, we captured a sequence of images $I(\theta_i, \theta_s)$. For each incident polarization set of angles $\{0°, 45°, 90°, 135°, 180°, 225°, 270°, 315°\}$, we took a pair of images corresponding to its parallel θ_s and perpendicular $\theta_s + 90°$ detections. In this way, we recorded sixteen images (8 parallel and 8 perpendicular images) for each sample with respect to the different angles of observation. Mueller matrix coefficient derivation has been described in the Table 2. Collection of images using MS_2 has been presented in Fig. 7.

2.3. Mueller matrix polarimetry

Polarimetry is the measurement technique, that can be applied for interpretation of the polarization of light. In general, when the light interacts with optical elements that include polarizers, filters, lenses surfaces, scattering media, etc, it can change the state of its polarization. This interaction with any optical element or material can be
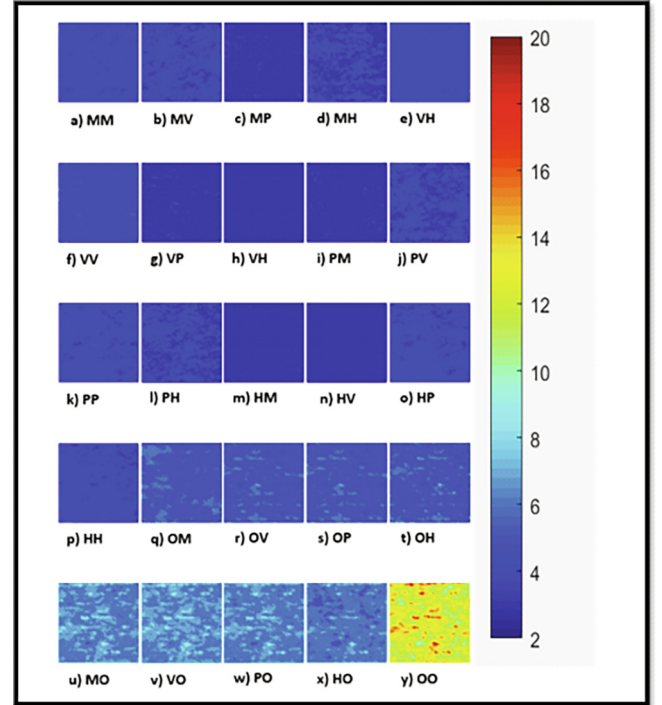
Fig. 6. Images for wood vertical with respect to the observation angles $10°$ using MS_1. The color bar represents the light intensity. By using these images, we can derive 3×3 Mueller matrix elements. Last image (y) shows high intensity of light rather than all other, because unpolarized light fall on the sample. From (p) to (x) images are more bright rather then others, because we have been recording these images using only one polarizer.

defined as a multiplication of the Stokes vector with a 4×4 matrix, $S' = MS$.

$$S = \begin{bmatrix} I \\ Q \\ U \\ V \end{bmatrix}$$

Stokes vector elements demonstrated as the total intensity of light I, the amount of linear horizontal or vertical polarization Q, the amount of linear $+45°$ or $-45°$ polarization U and the amount of right or left circular polarization contained in the light beam V. The stokes matrix is modified in terms of Mueller may be written as:

$$\begin{bmatrix} I_{out} \\ Q_{out} \\ U_{out} \\ V_{out} \end{bmatrix} = \begin{bmatrix} m_{11} & m_{12} & m_{13} & m_{14} \\ m_{21} & m_{22} & m_{23} & m_{24} \\ m_{31} & m_{32} & m_{33} & m_{34} \\ m_{41} & m_{42} & m_{43} & m_{44} \end{bmatrix} \begin{bmatrix} I_{inp} \\ Q_{inp} \\ U_{inp} \\ V_{inp} \end{bmatrix} \tag{1}$$

Thus, we work with the reduced matrix:

$$\begin{bmatrix} I_{out} \\ Q_{out} \\ U_{out} \end{bmatrix} = \begin{bmatrix} m_{11} & m_{12} & m_{13} \\ m_{21} & m_{22} & m_{23} \\ m_{31} & m_{32} & m_{33} \end{bmatrix} \begin{bmatrix} I_{inp} \\ Q_{inp} \\ U_{inp} \end{bmatrix} \tag{2}$$

Here, the elements of the input and output vectors may be written as:

$$\begin{bmatrix} I \\ Q \\ U \end{bmatrix} = \begin{bmatrix} H+V \\ H-V \\ M+P \end{bmatrix} \begin{bmatrix} I_{90}+I_0 \\ I_{90}-I_0 \\ I_{+45}+I_{-45} \end{bmatrix} \tag{3}$$

So, scattering matrix for an isotropic symmetric medium may be represented as:

Table 1

Polarization imaging for the Methodology Scheme MS_1.

Illuminations	Observations				
	315°(M)	0°(V)	45°(P)	90°(H)	N
315°(M)	1–315°(MM)	2–0°(MV)	3–45°(MP)	4–90°(MH)	21-N(MN)
0° (V)	5–315°(VM)	6–0°(VV)	7–45°(VP)	8–90°(VH)	22-N(VN)
45°(P)	9–315°(PM)	10–0°(PV)	11–45°(PP)	12–90°(PH)	23-N(PN)
90° (H)	13–315°(HM)	14–0°(HV)	15–45°(HP)	16–90°(HH)	24-N(HN)
N	17–315°(NM)	18–0°(NV)	19–45°(NP)	20–90°(NH)	25-N(NN)

Table 2

All elements from a to p in the given formulas are the images for the formation of Mueller matrix using MS_2. We have presented, these images from a to p illustrated in the Fig. 7.

	Mueller matrix elements formation for MS_2
m_{11}	$\frac{image(a)+image(b)+image(e)+image(f)+image(i)+image(j)+image(m)+image(n)}{2}$
m_{12}	$\frac{image(e)+image(f)+image(m)+image(n)}{4} - \frac{image(a)+image(b)+image(i)+image(j)}{4}$
m_{13}	$\frac{image(c)+image(d)+image(k)+image(l)}{4} - \frac{image(g)+image(h)+image(o)+image(p)}{4}$
m_{21}	$\frac{image(b)+image(e)+image(j)+image(m)}{2} - \frac{image(a)+image(f)+image(i)+image(n)}{2}$
m_{22}	$\frac{image(e)+image(m)+image(a)+image(i)}{8} - \frac{image(f)+image(n)+image(b)+image(j)}{8}$
m_{23}	$\frac{image(d)+image(l)+image(g)+image(o)}{8} - \frac{image(c)+image(k)+image(h)+image(p)}{8}$
m_{31}	$\frac{image(c)+image(h)+image(k)+image(p)}{2} - \frac{image(d)+image(g)+image(l)+image(o)}{2}$
m_{32}	$\frac{image(e)+image(f)+image(i)+image(j)}{8} - \frac{image(n)+image(m)+image(b)+image(a)}{8}$
m_{33}	$\frac{image(c)+image(g)+image(k)+image(o)}{8} - \frac{image(d)+image(h)+image(l)+image(p)}{8}$
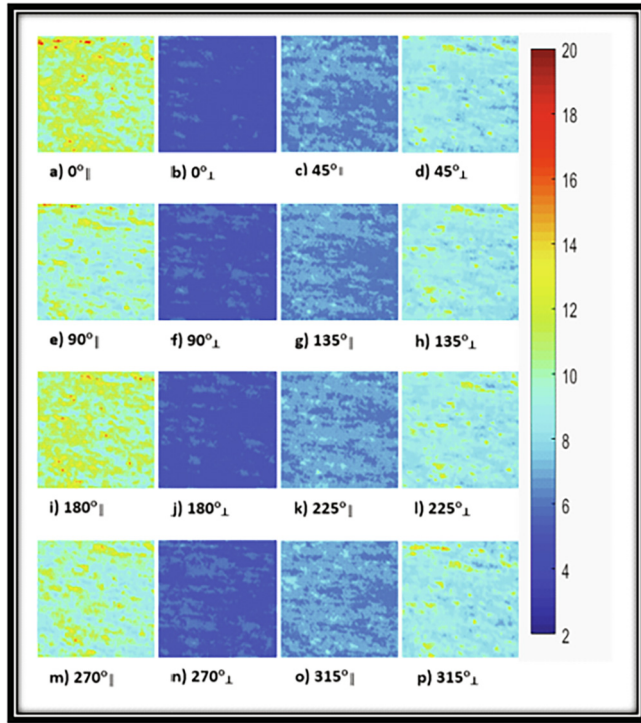
Fig. 7. Images for wood-H with respect to the observation angle 10° using MS_2, where subscripts $\parallel$ and $\perp$ corresponds to parallel and orthogonal components of respective angle. The color bar represents the light intensity input to the output.

$$\begin{bmatrix} m_{11} & m_{12} & 0 \\ m_{21} & m_{22} & 0 \\ 0 & 0 & m_{33} \end{bmatrix} \tag{4}$$

Symmetric homogeneous scattering gives the following condition:

$$m_{21} = m_{12} \tag{5}$$

As we are working on 3×3 Mueller matrix, so matrix for our case will become:

$$\begin{bmatrix} I_{out} \\ Q_{out} \\ U_{out} \end{bmatrix} = \begin{bmatrix} H+V \\ H-V \\ M+P \end{bmatrix} = \begin{bmatrix} m_{11} & m_{12} & 0 \\ m_{21} & m_{22} & 0 \\ 0 & 0 & m_{33} \end{bmatrix} \begin{bmatrix} I_{in} \\ Q_{in} \\ U_{in} \end{bmatrix} \tag{6}$$

Performing multiplications, we obtain:

$$I_{out} = m_{11}I_{in} + m_{12}Q_{in} \tag{7}$$

Substituting Eq. (5) in Eq. (7), we have:

$$I_{out} = m_{11}I_{in} + m_{21}Q_{in} \tag{8}$$

By substituting $I_{out} = H_o + V_o$, we get:

$$H_o + V_o = m_{11}(H_i + V_i) + m_{12}(H_i - V_i) \tag{9}$$
$$H_o - V_o = m_{12}(H_i + V_i) + m_{22}(H_i - V_i) \tag{10}$$

After simplification, we obtained:

$$H_0 = \left(\frac{m_{11} + 2m_{12} + m_{22}}{2}\right)H_i + \left(\frac{m_{11} - m_{22}}{2}\right)V_i \tag{11}$$

$$V_0 = \left(\frac{m_{11} - m_{22}}{2}\right)H_i + \left(\frac{m_{11} - 2m_{12} + m_{22}}{2}\right)H_i \tag{12}$$

This means that, illumination with H polarization, the output is on both polarizations:

$$H_0 = \left(\frac{m_{11} + 2m_{12} + m_{22}}{2}\right)H_i \tag{13}$$

$$V_0 = \left(\frac{m_{11} - m_{22}}{2}\right)H_i \tag{14}$$

Similarly illumination with V polarization the output can be detected again on both polarizations:

$$H_0 = \left(\frac{m_{11} - m_{22}}{2}\right)V_i \tag{15}$$

$$V_0 = \left(\frac{m_{11} - 2m_{12} + m_{22}}{2}\right)V_i \tag{16}$$

2.4. Wood analysis

For the illumination with V/H polarization, we obtained a Mueller matrix similar to symmetrical and homogeneous one. Moreover, if $m_{12} \neq m_{21}$, the decomposition on polarization becomes:

$$H_0 = \left[\frac{m_{11} + m_{12} + m_{21} + m_{22}}{2}\right]H_i + \left[\frac{(m_{11} + m_{21}) - (m_{12} + m_{22})}{2}\right]V_i \tag{17}$$

$$V_0 = \left[\frac{(m_{11} + m_{12}) - (m_{21} + m_{22})}{2}\right]H_i + \left[\frac{(m_{11} + m_{22}) - (m_{12} + m_{21})}{2}\right]V_i \tag{18}$$

which means, illumination with H polarization, the output is on both polarizations, we obtained:

$$H_0 = \left[\frac{m_{11} + m_{12} + m_{21} + m_{22}}{2}\right] H_i$$

$$V_0 = \left[\frac{(m_{11} + m_{12}) - (m_{21} + m_{22})}{2}\right] H_i$$

and:

$$H_0 = \left[\frac{(m_{11} + m_{21}) - (m_{12} + m_{22})}{2}\right] V_i$$

$$V_0 = \left[\frac{(m_{11} + m_{22}) - (m_{12} + m_{21})}{2}\right] H_i$$

3. Physical interpretation of Mueller matrix coefficients

If the Mueller matrix elements are all unknown, they can be determined experimentally with different orientations of polarizers. The element m_{11} gives the information of the unpolarized light input to output intensity, so this factor can be interpreted as a simple transmission. m_{12} is obtained by measuring the total reflected intensity for horizontal input polarization and subtracting the total reflected intensity for vertical input polarization from it. m_{12} can be expressed as the Linear Extinction (LE) at 0°/90°. Similarly, m_{21} refers to degree of linear polarization of the scattered light; m_{22} refers the depolarization of input polarization. m_{23} is obtained by measuring the horizontal and vertical 0°/90° reflected intensity for an oblique input polarization. m_{23} and m_{32} express the Circular Retardance (CR) with opposite sign. In our experiment, we investigated the 3 × 3 Mueller matrix, for the characterization of selected samples at observation angle θ_s varying from 10° to 70°. We have taken an average of three repeated measurements for each sample and normalized all the obtained matrix elements.

During our numerical tests and elaborations, we have investigated the following features of each sample as illustrated in Figs. 8–10. First, we can see that the Mueller matrices for isotropic and anisotropic
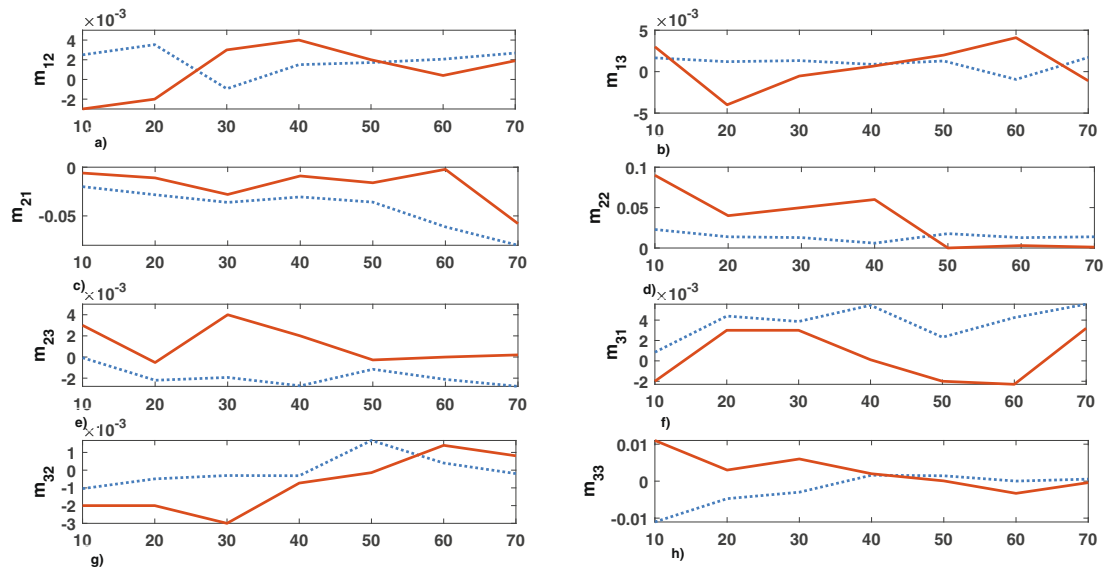
Fig. 8. Mueller Matrix elements M_{ij} for Teflon as functions of the observation angles. Red line represents the MS_1 scheme and blue dot line represents the MS_2 scheme.
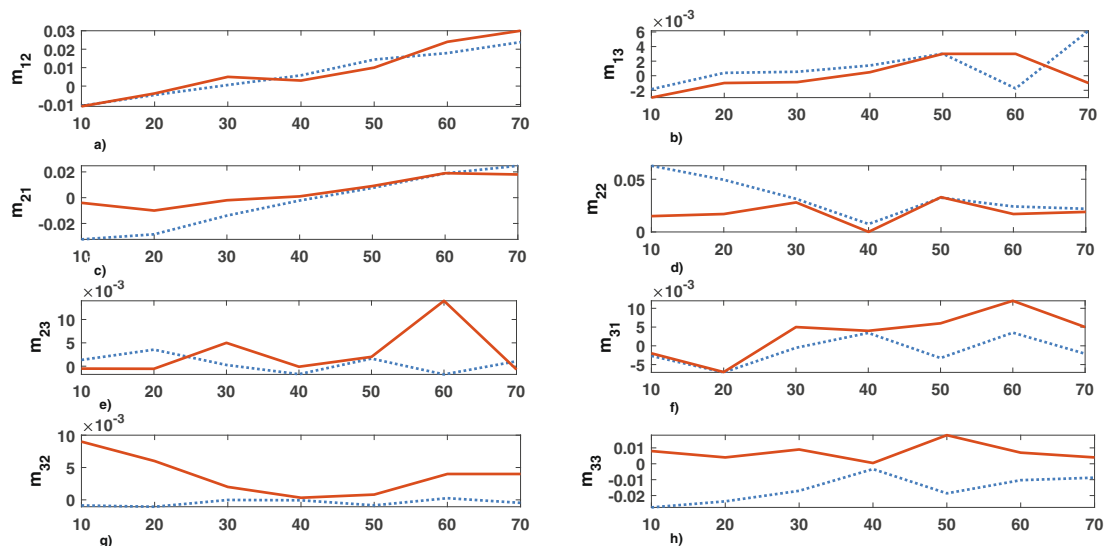
Fig. 9. Mueller Matrix elements M_{ij} for wood-H as functions of the observation angles. Red line represents the MS_1 scheme and blue dot line represents the MS_2 scheme.
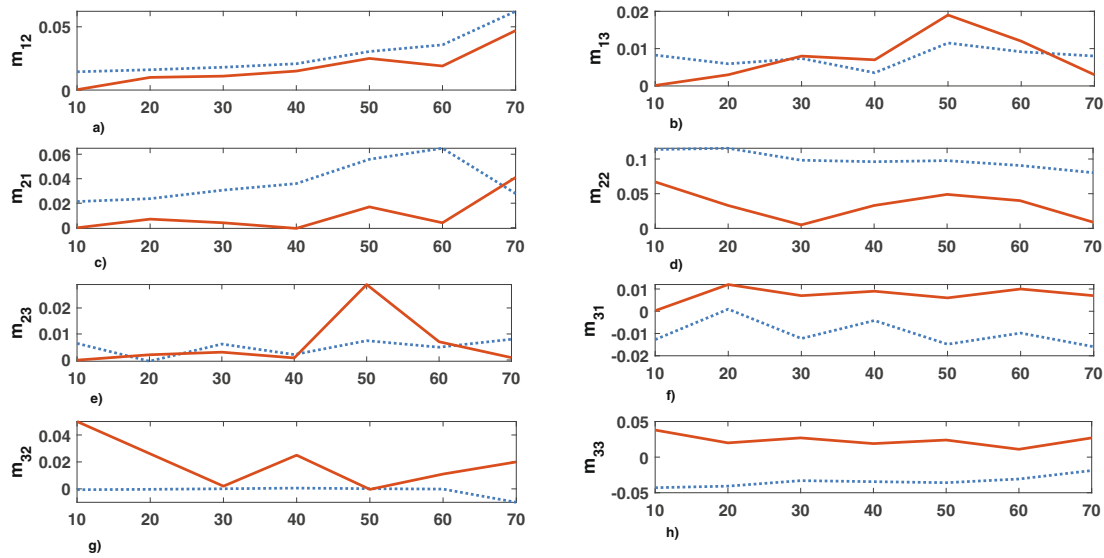
Fig. 10. Mueller Matrix elements M_{ij} for wood-V as functions of the observation angles. Red line represents the MS_1 scheme and blue dot line represents the MS_2 scheme.
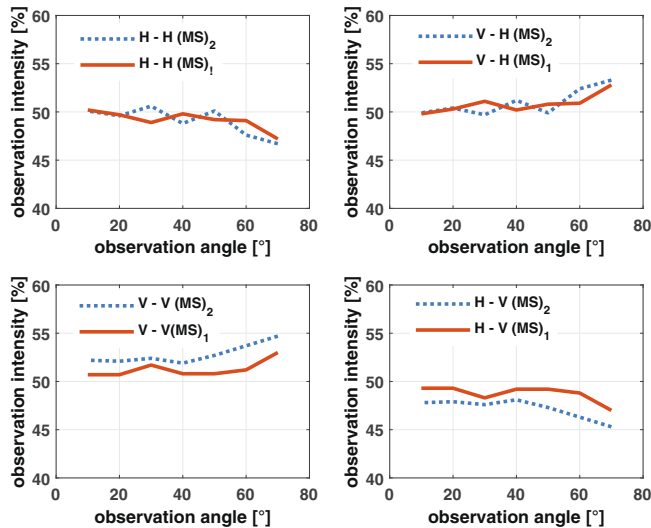
Fig. 11. The output to input intensity for Teflon using both formations MS_1 and MS_2.

Fig. 12. The output to input intensity for wood-V using both formations MS_1 and MS_2.

samples are non-diagonal, employing both formations MS_1 and MS_2. Further, the magnitude of the diagonal elements m_{22} and m_{33} is not equal. In order to identify the alignment of the fibers in anisotropic samples, we have inspected the signs and values of all matrix elements. For the case of wood sample fibers are distributed along both orientations (horizontal and vertical), leading to a larger value of the diagonal elements m_{22} and m_{33}. Comparison between the Figs. 8–10, also reveals some distinctive differences between the Teflon, wood-H, and wood-V samples.

For example, the Teflon has smaller diagonal elements m_{22} and m_{33} as compared to both wood-H and wood-V samples. Wood-V has higher value of diagonal elements m_{22} and m_{33} as compared to wood-H. The abundance of cellulose in wood is the cause of notable absorption, and results in larger values of diagonal elements of wood as compared to the Teflon. For the anisotropic wood-H and wood-V samples, m_{22} and m_{33} have different values in the entire range of observation angles.

m_{13}, m_{23}, m_{31}, and m_{32} are approaching zero in analysis of the Teflon and wood-H samples (see Figs. 8, 9, b, e, f, g). But for the case of wood-V, these elements display minimum values rather than zero (see Figs. 10, b, e, f, g). It can be seen that m_{22} is more sensitive for the identification of the wood-V, wood-H and Teflon samples. For instance: for the case of Teflon with MS_2 formation, the value of m_{22} is decreasing with increasing observation angle from $10°$ to $40°$. Observed lowest value is at $40°$. From $40°$ to $70°$, it is rising randomly at different angles. Similarly, Teflon with MS_1 formation, m_{22} shows fluctuations for entire range of observation angle. And its value is approaching to zero at $50°$ (see Fig. 8 d).

For the case of wood-H, m_{22} has higher magnitude as compared to Teflon but its graphical presentation across the whole observation is similar to Teflon (see Fig. 9 d). Using both formations (MS_1 and MS_2), m_{22} approaches to zero at $40°$ observation angle. For the case of wood-V, m_{22} has higher value as compared to Teflon and wood-H, but it presents irregular behavior for all observation angles (see Fig. 10 d).
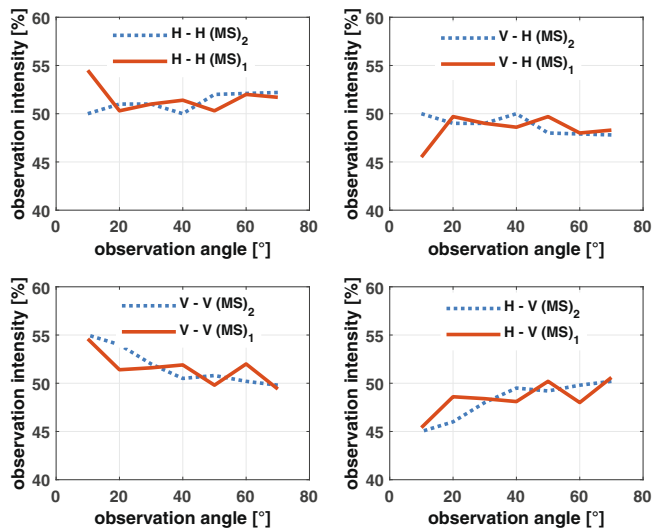
Fig. 13. The output to input intensity for wood-H using both formations MS_1 and MS_2.

For validation of results, we have investigated and compared both formation schemes MS_1 and MS_2. This information confesses us to conclude that the change in polarization state of light after interaction with wood fibers plays significant role, which can also contribute in its detection. Wood-V has more significant numerical results than wood-H and Teflon. We can say that wood-V shows more sensitiveness towards the polarization state of light. Teflon is isotropic in general as it has no texture, so it is independent of orientation. We can say that it does not depict active response towards any polarization state.

3.1. Numerical results and discussion

We have presented the results of Mueller matrix measurements for three different samples using two different approaches MS_1 and MS_2. Samples include wood-H and wood-V and Teflon. Introduced schemes record images for different combinations of input polarization and output detection. We calculated output to input intensity using Eqs. (19)–(22) for all samples and results obtained from both schemes. Fig. 11, presents the obtained results for Teflon. It shows that for both input polarizations (horizontal and vertical), output to input intensity converges to almost 50%. But few fluctuations are still present that can be approximated as a result of human errors. Fig. 12, shows the obtained results for wood-V. When input polarization is horizontal then output to input intensity is more prominent and it has higher percentage as compared to the input vertical polarization. Fig. 12, is the representation of output to input intensity for wood-H. We can see that output to input intensity depends on input polarization, such that for any of the input polarization states, it increases up to the similar value only if the input and output detection has same state of polarization. Likewise, for cross detection (H-V, V-H), the decrease in value of intensity is also similar for any input polarization. In general, for same input polarization and output detection (H-H, V-V), the magnitude of output to input intensity is higher than cross detection (H-V, V-H). We can also see that in both presented formation schemes, obtained results are close to each other which allows us to say that there are fewer chances of errors. (See Fig. 13)

3.2. Conclusions

In this paper, we apply polarization imaging technique on wood-H, wood-V and Teflon samples. Wood-H and wood-V demonstrates differ-

ent anisotropic material samples whereas Teflon demonstrates isotropic material sample. Using 3×3 Mueller matrix, we calculated values corresponding to polarization parameters that are Linear Extinction (LE), Depolarization (D), Circular Retardance (CR), and Transmission (T). These parameters are used to identify the characteristic features of the selected samples.

For better results, we introduced two different formations MS_1 and MS_2 to examine the relationship between structural parameters of Mueller matrix and physical and morphological structure of samples. The graphical representation of all Mueller matrix elements using both formations MS_1 and MS_2 shows the same trend of variation with respect to observation angles. It means, both formations are valid for sample characterization. We can say that MS_2 is simpler, more efficient and shorter so it will be more attractive to the user.

The experimental and simulation results confirm that the Mueller matrix element m_{22} is more sensitive for the entire range of observation angles in all samples compared to other elements. We derived the ratio of output to input intensity using matrix elements and we calculated it for all samples. Our analysis shows that isotropic Teflon has nearly equal output to input intensity. Whereas for anisotropic wood samples output to input intensity depends on input polarization.

In future, we propose to extend these derived formations for arteries, nerves, and veins. We are considering isotropic Teflon is similar to veins in humans, as veins do not have any fibrous structures on its surface. Arteries have fibers along their circumference, we are manifesting wood-H as an artery. We are considering wood-V as nerves, because they have longitudinal fibers.

Funding

Declaration of Competing Interest

The authors declare that they have no known competing financial interests or personal relationships that could have appeared to influence the work reported in this paper.

References

Alali, S., Vitkin, I.A., 2015. Polarized light imaging in biomedicine: emerging Mueller matrix methodologies for bulk tissue assessment. J. Biomed. Opt. 26, 061104.

Batool, S., Naqvi, Q.A., Fiaz, M.A., 2018. Scattering from a cylindrical obstacle deeply buried beneath a planar non-integer dimensional dielectric slab using Kobayashi potential method. Optik 153, 95–108.

Batool, S., Frezza, F., Mangini, F., Xu, Y.L., 2020a. Scattering from multiple PEC sphere using translation addition theorems for spherical vector wave function. J. Quant. Spectrosc. Radiat. Transf. 248, 106905.

Batool, S., Frezza, F., Mangini, F., Simeoni, P., 2020b. Introduction of radar scattering application in remote sensing and diagnostics. Atmosphere 11, 517–533.

Batool S., Nisar M., Mangini F., Frezza F., Fazio E., 2020. Polarization Imaging for Identifying the Microscopical Orientation of Biological Structures, 33rd General Assembly and Scientific Symposium of the International Union of Radio Science, URSI GASS, 29 Aug 2020..

Batool, S., Nisar, M., Mangini, F., Frezza, F., Fazio, E., 2020d. Scattering of light from the systemic circulatory system. Diagnostics 10, 1026.

Sidra B, Mehwish N, Fabio M, Fabrizio F, Eugenio F. Interpreting Mueller matrix of anisotropic material. In 2021 15th European Conference on Antennas and Propagation (EuCAP) 2021 Mar 22 (pp. 1–4). IEEE. https://ieeexplore.ieee.org/abstract/document/9411171?casa_token=0D0Cm_fgY0wAAAAA:32u4noa7Fa3OBQ8uKhVvZQPbfUvAdYIlm6g-HRS4M8QUaXDp1BlwjEC-nr-CWLJSq1jq8wg.

De Boer, J.F., Milner, T.E., 2002. Review of polarization sensitive optical coherence tomography and Stokes vector determination. J. Biomed. Opt. 7, 359–372.

Demos S., Staggs M.C., 2006. inventors., Near-infrared spectroscopic tissue imaging for medical applications. United States patent no 7, 717, (2006)..

Fratzl, P., Jakob, H.F., Rinnerthaler, S., Roschger, P., Klaushofer, K., 1997. Position-resolved small-angle X-ray scattering of complex biological materials. J. Appl. Crystallogr. 30, 765–769.

Fujimoto, J.G., Farkas, D., 2009. Biomedical Optical Imaging. Oxford University Press.

Gurjar, R.S., Backman, V., Perelman, L.T., Georgakoudi, I., Badizadegan, K., Itzkan, I., Dasari, R.R., Feld, M.S., 2001. Imaging human epithelial properties with polarized light-scattering spectroscopy. Nat. Med. 7, 1245–1248.

Jacques, S.L., Roman, J.R., Lee, K., 2009. Imaging superficial tissues with polarized light. Lasers in Surgery and Medicine, J. Am. Soc. Las. Med. Sur. 26, 119–129.

Jacques, S.L., Roussel, S., Samatham, R.V., 2016. Polarized light imaging specifies the anisotropy of light scattering in the superficial layer of a tissue. J. Biomed. Opt. 21, 071115.

Jiao, S., Wang, L.V., 2002. Jones-matrix imaging of biological tissues with quadruple-channel optical coherence tomography. J. Biomed. Opt. 7, 1083–3668.

Johnson, C.C., Guy, A.W., 1972. Nonionizing electromagnetic wave effects in biological materials and systems. Proc. IEEE 60, 692–718.

Kienle A., D Andrea C., Foschum F., Taroni P., Pifferi A., 2008. Light propagation in dry and wet softwood. Opt. Expr., 16 9895-906..

Layden, D., Ghosh, N., Vitkin, A., 2013. Quantitative polarimetry for tissue characterization and diagnosis. Adv. Biopho. Tis. Opt. 5, 73–108.

Liu, C.H., Das, B.B., Glassman, W.S., Tang, G.C., Yoo, K.M., Zhu, H.R., Akins, D.L., Lubicz, S.S., Cleary, J., Prudente, R., Celmer, E., 1992. Raman, fluorescence, and time-resolved light scattering as optical diagnostic techniques to separate diseased and normal biomedical media. J. Photochem. Photobiol. B 16, 187–209.

Mangini, F., Tedeschi, N., 2017. Scattering of an electromagnetic plane wave by a sphere embedded in a cylinder. J. Opt. Soc. Am. A 34, 760–769.

Saarinen, Kari, Muinonen, Karri, 2011. Light scattering by wood fibers. Appl. Opt. 40, 5064–5077.

Tuchin, V.V., 2016. Polarized light interaction with tissues. J. Biomed. Opt. 21, 071114.

Vo, Dinh T., 2014. Biomedical Photonics Handbook: Biomedical Diagnostics. CRC Press.

Yu, X., Zhang, S., Olivo, M., Li, N., 2020. Micro-and nano-fiber probes for optical sensing, imaging, and stimulation in biomedical applications. Photon. Res. 8, 1703–1724.

Zaffar, M., Pradhan, A., 2020. Assessment of anisotropy of collagen structures through spatial frequencies of Mueller matrix images for cervical pre-cancer detection. Appl. Opt. 59, 1237–1248.